2011 International Conference on Bioscience, Biochemistry and Bioinformatics
IPCBEE vol.5 (2011) © (2011) IACSIT Press, Singapore

A Multiscale Model for Hypoxia-induced Avascular Tumor Growth

Xuefeng Gao
Computer Science Dept
University College Cork
Cork, Ireland
e-mail: xfg1@cs.ucc.ie

Mark Tangney
Cork Cancer Research Centre
University College Cork
Cork, Ireland
e-mail: m.tangney@ucc.ie

Sabin Tabirca
Computer Science Dept
University College Cork
Cork, Ireland
e-mail: tabirca@cs.ucc.ie

***Abstract*—We present a cell-based multiscale model for avascular tumor growth aimed at investigating the tumor morphology under hypoxia condition. At the extracellular level, the diffusion of oxygen, glucose and hydrogen ions describe the chemical dynamics involved in metabolism. At the cellular level, a *Glazier-Graner-Hogeweg* (GGH) model describes cellular dynamics including cell proliferation, viability and adhesion. At the subcellular level, the expression of protein p27 regulates the cell cycle. In this model each tumor cell reacts to the local environment by changing its phenotype. For example, tumor cells can adapt to the low oxygen concentration in the tissue by undergoing anaerobic metabolism. In particular, we have analyzed cancer cells can undergo quiescence (G_0 phase in the cell cycle) by increasing their levels of p27, which increase their survival chances in hypoxia situation. This model produces a layered structure avascular tumor that quantitatively in agreement of B16F10 melanoma in vivo experiment measurements.**

Keywords-avascular Tumor; hypoxia; p27 expression; GGH model; multiscale

I. INTRODUCTION

A. Biology Background

Tumor evolution is a complex phenomenon involving many interrelated processes across a wide range of spatial and temporal scales. Solid tumors are known to progress through two distinct phases of growth-the avascular phase and the vascular phase [14, 15]. Avascular growth refers to the initial, diffusion limited phase of a solid tumor during which the rate of tumor expansion depends on the critical nutrients (e.g. oxygen and glucose) diffusing into the tumor mass from the surrounding tissue. The nutrients become scarce rapidly due to the limited number of normal tissue vasculature present in the tissue. It is well documented that low oxygen concentrations (hypoxia) alter the progression of cell division cycle [19]. Normal and cancer cells response to hypoxia in remarkable different ways, whereas normal cells usually undergo apoptosis when the hypoxic stress is too intense or persists for too long, cancer cells exhibit higher resistance to hypoxia. However, cancer cells eventually die if the DNA is significant damaged. Plenty of research results have suggested that cancer cells undergo anaerobic metabolism in poor oxygen situation [25, 9]. Anaerobic glycolysis is less efficient at generating energy molecules (ATP) and produce lactic acid (H^+) as a by-product. Constitutive up-regulation of glycolysis is also observed even in the presence of adequate oxygen supplies, which was first observed by Warburg [5].

Cell cycle refers to the series of events that a eukaryotic cell has to proceed orderly in order to undergo division. Four distinct, ordered phases constitute a cell cycle: DNA synthesis (*S*) and mitosis (*M*) alternate with one another, separated by two "gap" phases (G_2 and G_1) of preparation and growth. If cells sense inadequate growth conditions (e.g. hypoxia) or receive inhibitory signals prior to the G_1/S transition (restriction point), they abandon normal progression and enter a resting state (G_0), also called quiescence. In this state, most of the cell functions are suspended, most notably, proliferation. Progression through the cell-division cycle is regulated by the coordinated activities of cyclin-dependent kinases (CDK) that are sequentially regulated by cyclins D, E, and A [26]. The CDKs induce downstream processes by phosphorylating selected proteins. However, to do this, they must be activated by binding to the cyclins. Cyclins undergo a cycle of synthesis and degradation parallel to the cell division cycle. One level of regulation of these cyclin-CDK complexes is provided by their binding to CDK inhibitors (CKIs). Two CKI gene families have been identified according to their evolutionary origins, structure, and CDK specificities [30]. Members of the INK4 (inhibitor of CDK4) family of CKIs (p15, p16, p18, and p20) inhibit the activity of both CDK4 and CDK6, while members of the Kip/Cip family of CKIs (p21, p27, and p57) inhibit specifically the activity of CDK2 by binding both to cyclin E/CDK2 and cyclin A/CDK2 complexes [37]. CDK network is very complex, for modeling purposes, we only take into account the p27 protein expression in regulating the G_1/S transition.

p27 are rarely found in human cancer cells [29]. According to Park *et al*.'s experiment report [27], p27 is produced as a regulator of cell proliferation [13]. p27 was shown to be induced by hypoxia, leading to G_1/S arrest [16, 19]. Upregulation of p27 induces cancer cell's ability to survive under hypoxic stress by entering a quiescent state (G_0). Hence, we assume that the p27 levels in cancer cells are high likely relative to oxygen concentration. We suppose that the machinery of tumor cell entering quiescent state is basically triggered when p27 is below some threshold value, and we estimate this threshold value ranges accounting for experimental observations.

B. Computational Background

Since cancer biology problems are intrinsically specific, heterogeneous and multi-scale, cancer modeling has employed a wide range of techniques depending on their biological focus. Most of the current models are hybrid (adaptive finite-element/level-set model [42], hybrid cellular automaton [18], Potts model [38], cell-centered off-lattice model [17]) since they integrate both continuous and discrete variables and are able to incorporate biological phenomena on various temporal and spatial scales. One of widely used cell-based model is *Glazier-Graner-Hogeweg* (GGH) model [4]. The GGH model is a cell-oriented framework for defining a biological structure consisting of the configuration of a set of generalized cells, each represented on a cell lattice as a domain of lattice sites sharing the same cell index, a set of internal cell states for each cell, and a set of auxiliary fields. The cellular dynamics of GGH is implemented based on an *Effective Energy* or *Hamiltonian* which encapsulates almost all interactions between modeling components. At extracellular level, a set of partial differential equations (PDEs) and boundary conditions are used to describe the evolution of the environment fields. At intracellular level, ordinary differential equations (ODEs) can be integrated to define certain cell behaviors which depend on such as genetic regulatory pathways. Recently, a preliminary integration of the GGH modeling environment Compucell3D [11] with a famous biochemical modeling tool Systems Biology Workbench [35] which allows enhanced construction of more comprehensive models at subcellular level.

In this paper, we present a cell-based multiscale model to simulate avascular tumor growth under hypoxia situation. This model focuses on describing dynamics of multicellular tumor mass growth that accounts for nutrient supply and cancer cell's ability of adapting to hypoxia environment. Starting with a single cancer cell, this model eventually produces a layer structured avascular tumor. This model also describes few interactions between cancer cells and the extra cellular matrix by switching from aerobic to anaerobic metabolism. We estimate and validate part of system parameters by comparing the simulation results with experiment data.

II. MATERIALS AND METHODS

A. The GGH Methodology

Our simulation of avascular growth models uses the *Glazier-Graner-Hogeweg* model (GGH), a lattice based, multi-cell, stochastic model which describes biological cells and their interactions in terms of *Effective Energies* and constraints. GGH models have been used to simulate tumor growth including the beginning spherical morphologies [23], tumor angiogenesis [38] and the malignant fingered tumors [39]. In GGH model, cells are spatially-extended domains, which reside on a collection of lattice sites (i.e. voxels) at locations $\vec{\imath}$, sharing the same cell index, σ. Each cell has an associated cell type, τ. The *Effective Energy*, E in our model, determines a cell's configuration, motility, adhesion, and response to extracellular signals. The *Effective Energy* in our simulation includes constant volume cells interacting via differential adhesion:

$$E = \sum_{\vec{\imath},\vec{\jmath}\ neighbors} J\left(\tau(\sigma(\vec{\imath})),\tau(\vec{\jmath})\right)\left(1-\delta(\sigma(\vec{\imath}),\sigma(\vec{\jmath}))\right) + \sum_{\sigma}\lambda_{Vol}(\tau)(v(\sigma)-V_t(\tau(\sigma)))^2 \quad (1)$$

where $v(\sigma)$ is the volume in lattice sites of cell σ which is constrained to be close to the target volume V_t, and $\lambda_{Vol}\tau$ is the inverse compressibility of cells of type τ. $J\left(\tau(\sigma(\vec{\imath})),\tau(\sigma(\vec{\jmath}))\right)$ is the contact energy per unit area between neighboring cells $\vec{\imath}$ and $\vec{\jmath}$. $-2\lambda_{Vol}(v(\sigma)-V_t)$ is the internal pressure in cell σ. To model cytoskeletally-driven cell motility, the cell lattice evolves through attempts by cells to extend their boundaries into neighboring cells' lattice sites, slightly displacing the neighboring cells which currently occupy those sites. This cell rearrangement dynamics is relaxational *Monte-Carlo-Boltzmann-Metropolis* dynamics [4, 20, 24]. For each step, we randomly select a cell boundary voxel and attempt to displace a randomly chosen neighboring cell's target voxel and calculate the *Effective Energy* change ΔE, if the source cell displaced the target cell at that voxel. If ΔE is negative, i.e., the change is energetically favorable, we accept it. If ΔE is positive, we accept the change with probability $P = e^{-\Delta E/T}$, where T denotes intrinsic cytoskeletally-driven motility. On an N sites lattice, N displacement attempts are made in one *Monte Carlo Step* (MCS).

To model the dynamics of chemical fields (nutrients, wastes etc) diffusing in the domain, a set of time-dependent partial differential equations (PDEs) are involved. The substrate diffuses and is consumed by the tumor cells at a constant rate per cell:

$$\frac{\partial c}{\partial t} = D_c\nabla^2 c + S_c f - C_c N(x) \quad (2)$$

where D_c, S_c and C_c are positive constants representing the substrate *c*'s diffusion constant, production rate and consumption rate per tumor cell respectively. This model contains only three chemical fields, which are oxygen, glucose and hydrogen ions.

Our model contains four tumor cell types: normal, hypoxic, quiescent and necrotic. Normal tumor cell becomes hypoxia when the local oxygen concentration $O(\vec{\imath})$, drops below hypoxic threshold O_{hy} and becomes necrotic when $O(\vec{\imath})$ drops below necrotic threshold O_{nc}. Normal and hypoxic cells consume oxygen and glucose to support their growth and proliferation. We assume that normal cells have same oxygen consumption rate C_o and glucose consumption rate C_g with hypoxic cells. Active tumor cells proliferate at a rate which depends on the oxygen partial pressure according

to a *Michaelis-Menten* form. We model a tumor cell's growth by increasing its target volume V_t at each MCS according to:

$$\frac{dV_t}{dt} = g_m \frac{O(\vec{i})}{O(\vec{i}) + P} \quad (3)$$

where g_m is the maximum growth rate, $O(\vec{i})$ is the oxygen concentration at center-of-mass of a cell and P is an positive control constant. The initial target volume for tumor cells isV_0. When a tumor cell reaches the doubling volume $V_d = 2V_0$, it divides and splits along a random axis into two tumor cells with equal initial target volumes V_0 [4]. Necrotic cells lose volume at a constant rate k. A zero volume cells will be removed from the system after a given time t_N. Some experiments suggest that the majority of cell death in spheroids occurs by necrosis [9]. In our model, cell death means strictly necrosis, we don't consider apoptosis. The extracellular medium (ECM) is a complex mixture of nondiffusing macromolecules which maintains the integrity of normal tissues. Different with tumor cells, we define ECM cell as a generalized, non-fully functional medium type of object. In our model, the ECM cells have low cellular motility and don't undergo normal cell cycle (don't divide, grow or die).

B. p27 Induced Cancer Cell Quiescence

In normal cells, hypoxia simply slows down the cell-cycle, whereas in cancer cells it induces both arrest and quiescence (G_0 phase) [16]. When cells go into a quiescent state, most of their functions, including proliferation, are suspended. The ability of cancer cells become quiescent provides them with a remarkable resistance to hypoxia [34]. In order to model the effect of hypoxia on the cell-cycle we consider a protein in the CDK network, protein p27, which inhibits DNA synthesis through inhabiting CDK2 activity and forestalling *S* phase entry through retinoblastoma protein hypophosphorylation [19].

Gardner *et al.* [19] have proposed mechanism for hypoxia induced cell-cycle arrest in normal cells (fibroblasts), based on which Alarcón *et al*. [6] have proposed a simplified version to investigate how p27 expression regulating cancer cell cycle. Building on these two models and experimental information on the effects of hypoxia on the cell-cycle, we create a mathematical model for hypoxia induced p27 production z of a single tumor cell by:

$$\frac{dz}{dt} = c_1 - c_2 \frac{O(\vec{i})}{K_{m1} + O(\vec{i})} z - M_m \frac{z}{K_{m2} + z} \quad (4)$$

where c_1 and c_2 control the production rate of p27, K_{m1} and K_{m2} are Michaelis constants, and M_m is the maximum decay velocity of p27. p27 dynamics depends on the oxygen tension, which is reset to initial value at each end of cell division. We assume that hypoxic tumor cells become quiescent when its p27 value rises above some threshold value Z_q.

C. Implementation and Parameters

Our model is implemented using the open-source CompuCell3D simulation environment [31]. The dimension of the 3D lattice domain in voxels is 90×90×90 with periodic boundary conditions. Each simulated tumor cell occupies a 27 voxels as initial volume V_0 . In our simulations, the initial size of a simulated tumor cell is 480 μm, which is about 60 times greater than the size of a real cell [32, 7].

It takes approximately 8h to 24h for a cell to progress through the entire cell-cycle once depending on the types of cells [2], and we chose an intermediate value 16h in this model. The conversation of a physical diffusion constant into a computational environment depends on the time and distance scales we choose. Abbas *et al*. [12] have used 1000 MCS ~ 24h as time scale in their simulations based on the speed of cell movement. Since the simulated tumor cells in our simulation are relatively stable in their positions, we chose 100 MCS ~ 24h. All cell species parameters and diffusion constants of related substrates have been measured experimentally and are summarized in TABLE I. .

The mechanism of this model consists of three scales: chemicals diffusing in extracellular level, cell cycle in cellular level and p27 expression in subcellular level. At each MCS, we first solve the PDEs to obtain the concentrations of metabolites for each cell, and then update the cell's target volume and its p27 expression based on current oxygen concentration. The cell reacts to its local environment in the following steps:

1) A normal tumor cell turns into hypoxic type if its oxygen concentration bellows O_{hp};

2) A normal or hypoxic cell becomes necrotic if its oxygen concentration bellows O_{nc} or its glucose concentration bellows G_{nc};

3) A hypoxic cell becomes quiescent if its p27 expression is above Z_q;

4) A quiescent cell turns into necrotic if its local oxygen concentration has fallen below O_{hp} for 3 days (300 MCS) or longer.

III. RESULTS

We start our simulation with a single generalized tumor cell near the center of the cubic lattice. Figure 1. shows the cross sections of the same tumor mass at different stages of growth: the initial proliferating cell aggregate, the onset of quiescence and the present of a necrotic domain. Figure 2. shows the growth curves of a solid tumor in comparison with experimental data of B16-F10 murine melanoma tumors growing in mice.

The tumor size was collected in cm^3 for 25 days after the mice were given by B16 cells. We use a medium tumor cellular density, 2.0×10^6 cells/cm^3, to estimate the cell amount. The tumor begins exponential growth after day 7 (Figure 2.). Due to diffusion limited oxygen cannot support the cells in the interior, hypoxic cells appear during 8 ~ 10 days and quiescent cells are observed 12 ~ 24h later. The necrotic domain forms around 18 ~ 20 days. The time at which this occurs depends on the initial oxygen concentration in the surrounding tissue.

Our model also reproduces the fact that p27 expression is upregulated in hypoxic tumor cells. In Figure 3. , the concentration of p27 grows over time until the control system is reset to its initial condition. This pattern is repeated cyclically each time the cell divides. We compare the p27 expression of normal and hypoxic cells over time, and estimate an appropriate range of threshold values over which cell enters G_0 phase. The chosen of this threshold value has a direct effect on the thickness of quiescence and necrosis domains, which we will discuss in more detail later. In addition, Figure 3. also shows how division time varies depending on oxygen concentration. With lower oxygen tension, the tumor cell cycle has been extended and eventually arrested when cell turning into quiescent.

IV. DISCUSSION

Our model produces a solid avascular tumor growth from a single generalized cancer cell during 25 days. Due to limited supply of oxygen, the simulated tumor presents a necrotic core at the center of the spheroid which is surrounded by proliferating and quiescent cells at the surface and intermediate layer respectively. This model demonstrates multiscale events of solid tumor growth as dynamics progress and also present how tumor cells adapt hypoxia by changing its phenotype from aerobic to anaerobic glycolysis. The outcomes of our simulation consistent with a clinical study of B16 F10 murine melanoma tumor in mice.

At the subcellular level, we have focused on the role of the protein p27 as a mediator of cell response to oxygen starvation, in particular hypoxia-induced arrest and quiescence. Analysis based on the cell-cycle, this model explains the part of cancer cell's ability of adapting hash environment. Our model successfully produces how oxygen concentration affects the expression of protein p27. This model is also successful in simulating p27 induced quiescence, in agreement with experimental observations [16, 19]. In addition, our simulation gives an appropriate range of p27 threshold value, above which cancer cell will turn into quiescent.

While our model is consistent with a number of experimental observations, it still far beyond to explain avascular growth in other aspects as well as possesses some shortcomings that require further refinement. First, our model should incorporate cell apoptosis, since all the cell death in our model undergoes necrosis when the level of oxygen or glucose below a threshold. Second, it does not include cell's behavior under acidity environment, and does not distinguish properly with cell cycle arrest with quiescence: in our simulation, cell will exit the normal cell cycle by entering G_0 phase as soon as the level of p27 is above Z_q. Biologically, the justification for this is that the cell can only become quiescent during G_1 phase. In our future work, we will add a mechanism to inspect the cell cycle phases for each cell. On the other hand, we will extent this model into cancer gene therapy modeling, where the dynamics of drug delivery agents will be incorporated.

REFERENCES

[1] A.R.A. Anderson, "A hybrid multiscale model of tumour invasion: evolution and the microenvironment", In: *Single-Cell-Based Models in Biology and Medicine*, Chapter I.1. Basel, Switzerland: Birkhauser-Verlag, 2007.

[2] P. Calabresi and P.S. Schein, *Medical Oncology*, *2 ed*, McGraw- Hill, New York, 1993.

[3] W.f. Ganong, *Review of Medical Physiology, 19th ed*, pp. 329, Appleton & Lange, New York, 1999.

[4] J.A. Glazier, A. Balter, and N.J. Poplawski, "Magnetization to morphogenesis: a brief history of the Glazier-Graner-Hogeweg model", In: Anderson, A.R.A., Chaplain, M.A.J., Rejniak, K.A. (Eds.), *Single-Cell-Based Models in Biology and Medicine*, pp. 79. Birkhauser, Basel, 2007.

[5] O. Warburg, "The metabolism of tumors", London: Constable Press, 1930.

[6] T. Alarcón, H.M. Byrne and P.K. Maini, "A mathematical model of the effects of hypoxia on the cell-cycle of normal cancer cells," *J. Theor. Biol.*, Vol. 229, pp. 395411, 2004.

[7] A.R.A Anderson, "A hybrid mathematical model of solid tumour invasion: the importance of cell adhesion," *Math. Med. Biol.*, Vol. 22, pp. 163, 2005.

[8] N.F. al-Baldawi and R.F. Abercrombie, "Cytoplasmichydrogen ion diffusion coefficient," *Biophys. J.*, Vol. 61, pp. 1470-1479, 1992.

[9] J.M. Brown, "Tumor microenvironment and the response to anticancer therapy," *Cancer Biol. Ther.*, Vol. 1, pp. 453-458, 2002.

[10] J.J. Casciari, S.V. Sotirchos, and R.M. Sutherland, "Variation in tumour cell growth rates and metabolism with oxygen concentration, glucose concentration and extra-cellular pH," *J. Cell. Physiol.*, Vol. 151, pp. 386-394, 1992.

[11] R. Chaturvedi, C. Huang, B. Kazmierczak, T. Schneider, J.A. Izaguirre, T. Glimm, H.G.E. Hentschel, J.A. Glazier, S.A. Newman, and M.S. Alber, "On multiscale approaches to three-dimensional modeling of morphogenesis," *J. R. Soc. Interface*, Vol. 2, pp. 237-253, 2005.

[12] D.M. Cochran, D. Fukumura, M. Ancukiewicz, P. Carmeliet, and R.K. Jain, "Evolution of Oxygen and Glucose Concentration Profiles in a Tissue-Mimetic Culture System of Embryonic Stem Cells," *Ann. Biomed. Eng.*, Vol. 34, pp. 1247-1258, 2006.

[13] M.L. Fero, M. Rivkin, M. Tasch, P. Porter, C.E. Carow, E. Firpo, K. Polyak, L.H. Tsai, V. Broudy, R.M. Perlmutter, K. Kaushansky, and J.M. Roberts, "A syndrome of multiorgan hyperplasia with features of gigantism, tumorigenesis, and female sterility in p27 (Kip1)-deficient mice," *Cell*, Vol. 85, pp. 733-744, 1996.

[14] J. Folkman, "The vascularization of tumours," *Sci. Am.*, Vol. 234, pp. 58-73, 1976.

[15] J. Folkman, "Tumor angiogenesis," *Adv. Cancer Research*, Vol. 43, pp. 175-203, 1985.

[16] J. O. Funk, "Cancer cell cycle control," *Anticancer Res.*, Vol. 19, pp. 4772-4780, 1999.

[17] J. Galle, M. Hoffmann, and G. Aust, "From single cells to tissue architecture-a bottom-up approach to modelling the spatio-temporal organisation of complex multi-cellular systems," *J. Math. Biol.*, Vol.58, pp.261-283, 2009.

[18] X.F. Gao, M. Tangney, S. Tabirca, "2D simulation and visualization of tumour growth based on discrete mathematical models," In: ICBBT 2010, pp. 35-41, 2010.

[19] L.B. Gardner, Q. Li, M.S. Park, W.M. Flanagan, G.L. Semenza, and C.V. Dang, "Hypoxia inhibits G_1/S transition through regulation of p27 expression," , *J. Biol. Chem.*, Vol. 276, pp. 7919-7926, 2001.

[20] J.A. Glazier and F. Graner, "Simulation of the differential adhesion driven rearrangement of biological cells," *Phys. Rev.*, Vol. E 47, pp. 2128-2154, 1993.

[21] G. Helmlinger, F. Yuan, M. Dellian, and R.K. Jain, "Interstitial pH and pO2 gradients in solid tumors in vivo: high-resolution measurements reveal a lack of correlation," *Nature Medicine*, Vol. 3, pp. 177-182, 1997.

[22] E. Jahde, T. Volk, A. Atema, L.A. Smets, G. Karl-Heinz, and M.F. Rajewsky, "pH in human tumor xenografts and transplanted rat tumors: effect of insulin, inorganic phosphate, and m-iodobenzylguanidine," *Cancer Research*, Vol. 52, pp. 6209-6215, 1992.

[23] Y. Jiang, J. Pjesivac-Grbovic, C. Cantrell, and J.P. Freyer, "A multiscale model for avascular tumor growth," *Biophys. J.*, Vol. 89, pp. 3884-3894, 2005.

[24] N. Metropolis, A.W. Rosenbluth M.N., Rosenbluth, A.H. Teller, and E. Teller, "Equation of state calculations by fast computing machines," *J. Chem. Phys.*, Vol. 21, pp. 1087, 1953.

[25] W. Mueller-Klieser, "Tumor biology and experimental therapeutics," *Crit Rev Oncol Hematol,* Vol. 36, pp. 123-139, 2000.

[26] E.A. Nigg, "Cyclin-dependent protein kinases: key regulators of the eukaryotic cell cycle," *Bioessays*, Vol. 17 (6), pp. 471-480, 1995.

[27] K.H. Park, J.Y. Seol, T.Y. Kim, C.G. Yoo, Y.W. Kim, S.K. Han, Y.S. Shim, and C.T. Lee, " An adenovirus expressing mutant p27 showed more potent antitumor effects than adenovirus-p27 wild type," *Cancer Research*, Vol. 61, pp. 6163-6169, 2001.

[28] A. Patel, E.T. Gawlinski, S.K. Lemieux, and R.A. Gatenby, "A cellular automaton model of early tumor growth and invasion: the effects of native tissue vascularity and increased anaerobic tumor metabolism," *J. Theor. Biol.* , Vol. 213, pp. 315-331, 2001.

[29] J. Philipp-Staheli, S.R. Payne, and C.J. Kemp, "p27(Kip1): regulation and function of haploinsufcient tumour supressor and its misregulation in cancer," *Genes Dev.*, Vol. 13, pp. 1501-1512, 1999.

[30] J. Pines, "Cyclin-dependent kinase inhibitors: the age of crystals," *Biochim. Biophys. Acta*, Vol. 1332, M39-M42, 1997.

[31] N.J. Poplawski, A. Shirinifard, M. Swat, and J.A. Glazier, "Simulation of single-species bacterial biofilm growth using the Glazier-Graner-Hogeweg model and the CompuCell3D modeling environment," *Math. Biosci. Eng.*, Vol. 5, pp. 355, 2008.

[32] N.J. Poplawski, U. Agero, J.S. Gens, M. Swat, J.A. Glazier, and A.R. Anderson, "Front instabilities and invasiveness of simulated avascular tumors," *Bull. Math. Biol.*, Vol. 71, pp. 1189-227, 2009.

[33] J. Rohzin, M. Sameni, G. Ziegler, and B.F. Sloane, "Pericellular pH affects distribution and secretion of cathepsin B in malignant cells," *Cancer Research*, Vol. 54, pp. 6517-6525, 1994.

[34] J.A. Royds, S.K. Dower, E.E. Qwarnstrom, and C.E. Lewis, "Iponse of tumour cells to hypoxia: role of p53 and NFkB," *J. Clin. Pathol. Mol. Pathol.*, Vol. 51, pp. 55-61, 1998.

[35] H.M. Sauro, M. Hucka, A. Finney, C. Wellock, H. Bolouri, J. Doyle, and H. Kitano, "Next generation simulation tools: the systems biology workbench and biospice integration," *OMICS*, Vol. 7(4), pp. 355-372, 2003.

[36] P.A. Schornack and R.J. Gillies, "Contributions of cell metabolism and H diffusion to the acidic pH of tumors," *Neoplasia*, Vol. 5, pp. 135-145, 2003.

[37] C.J. Sherr and J.M. Roberts, "CDK inhibitors: positive and negative regulators of G_1-phase progression," *Exp. Cell Res.*, Vol. 264, pp. 148-168, 2001.

[38] A. Shirinifard, J.S. Gens, B.L. Zaitlen, N.J. Poplawski, M. Swat, and J.A. Glazier, "3D Multi-cell simulation of tumor growth and angiogenesis," *PLoS ONE*, Vol. 4, e7190, 2009.

[39] S. Turner, J.A. Sherratt, and D. Cameron, "Tamoxifen treatment failure in cancer and the nonlinear dynamics of TGFβ," *J. Theor. Biol.*, Vol. 229, pp. 101-111, 2004.

[40] P.W. Vaupel and M. Hockel, "Oxygenation status of human tumors: A reappraisal using computerized pO2 histography," In: P.W. Vaupel, D.K. Kelleher, and M. Gunderoth (Eds), *Tumor Oxygenation*, pp. 219-232, Gustav Fischer Verlag, Germany, 1995.

[41] P. Vaupel, F. Kallinowski, and P. Okunieff, "Bloodow, oxygen and nutrient supply, and metabolic microenvironment of human tumors: a review," *Cancer Research*, Vol. 49, pp. 6449-6465, 1989.

[42] X. Zheng, S.M. Wise, and V. Cristini, "Nonlinear simulation of tumor necrosis neo-vascularization and tissue invasion via an adaptive finite-element/level-set method," *Bull. Math. Biol.*, Vol. 67, pp. 211-259, 2005

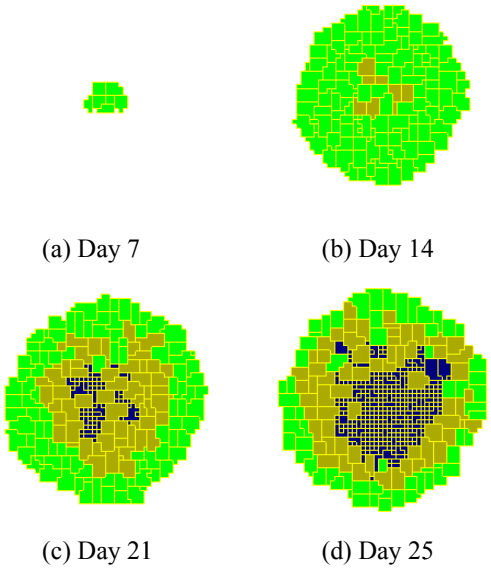

Figure 1. The cross-sectional view of a spheroid at different stages of development. (Green: proliferating region; Yellow: quiescent region; Blue: necrotic core.)

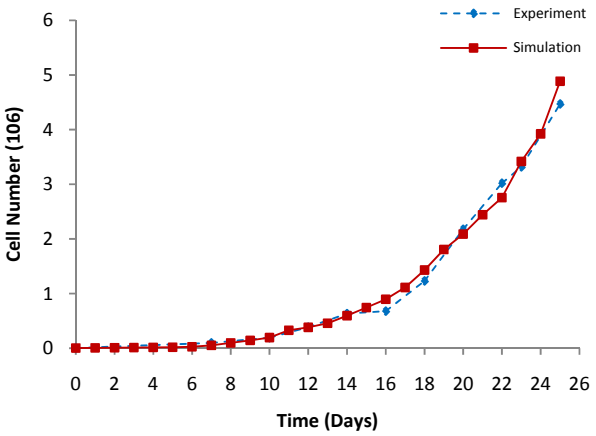

Figure 2. Growth curve of the simulated tumor comparing with B16 F10 murine melanoma tumor in mice. The solid line corresponds to B16 F10 tumor growth curve whereas the dashed line corresponds to the simulated tumor growth curve.

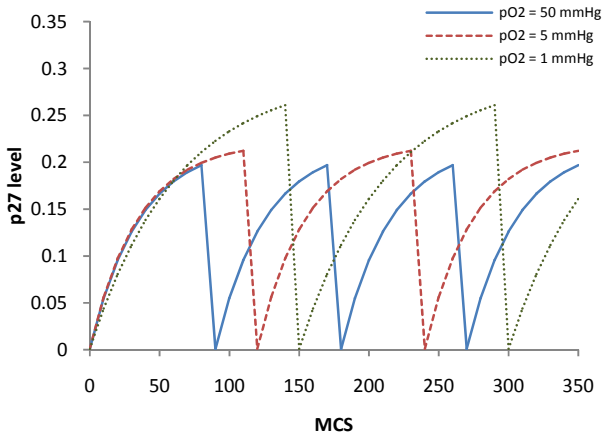

Figure 3. Diagram showing how levels of p27 expression varies for the normal and hypoxic cancer cells at different oxygen tensions.

TABLE I. A SUMMARY OF THE CELL SPECIFIC PARAMETERS AND MICRO-ENVIRONMENT SPECIFIC PARAMETERS

Variable	Biological Quantity	Value	References
V_0	Tumor cell initial volume	27 voxel	
V_d	Tumor cell doubling volume	54 voxel	
g	Maximum growth rate of individual cell	0.15-0.3	
C_o	Base oxygen consumption rate	8.28×10^{-13} mol cells^{-1}h^{-1}	[12]
C_g	Aerobic glucose consumption rate	1.368×10^{-13} mol cells^{-1}h^{-1}	[12]
C_g^a	Anaerobic glucose consumption rate	2.484×10^{-12} mol cells^{-1}h^{-1}	[1]
S_h	Hydrogen production rate	5.4×10^{-15} mol cells^{-1}h^{-1}	[21]
O_{hp}	Hypoxia oxygen threshold	3.28×10^{-9} mol cm^{-2}	[21]
O_{nc}	Necrosis oxygen threshold	1.12×10^{-9} mol cm^{-3}	[3]
D_c	Oxygen diffusion constant	6.48×10^{-2} cm^{2}h^{-1}	[12]
D_g	Glucose diffusion constant	3.96×10^{-2} cm^{2}h^{-1}	[12]
D_h	Hydrogen ion diffusion constant	3.96×10^{-2}cm^{2}h^{-1}	[8]
O_0	Oxygen background concentration	40-60 mm Hg	[29]
G_0	Glucose background concentration	6±1 mM	[22]
H_0	H^+ background concentration	3.98×10^{-11} mol cm^{-3} pH=7.4	[10]
Z_p	p27 induced quiescence threshold	0.21-0.23	
C_1	Control factor in Eq.(4)	0.01	
C_2	Control factor in Eq.(4)	0.007	
K_{m1}	Michaelis constant in Eq.(4)	0.01	
K_{m2}	Michaelis constant in Eq.(4)	100	
M_m	Maximum decay velocity of p27	0.01	
t_N	Necrotic cell removal rate	1-3 cell cycles	